Seismic Recording on Drifting Icebergs: Catching Seismic Waves, Tsunamis and Storms from Sumatra and Elsewhere

Emile A. Okal
Department of Geological Sciences, Northwestern University

Douglas R. MacAyeal
Department of the Geophysical Sciences, University of Chicago

INTRODUCTION

Under the Incorporated Research Institutions for Seismology (IRIS) Program for Array Seismic Studies of the Continental Lithosphere (PASSCAL) project SOUTHBERG, we have operated for the past three years a number of seismic stations on giant Antarctic icebergs parked or drifting slowly along the margins of the Ross Sea. The purpose of this deployment was to investigate *in situ* the characteristics and origin of high-frequency tremors emanating from inside the icebergs, tremors that previously had been detected in the far field as hydroacoustic T phases recorded in French Polynesia (Talandier *et al.* 2002, 2006). Similar observations were made later in the Indian Ocean by Chapp *et al.* (2005).
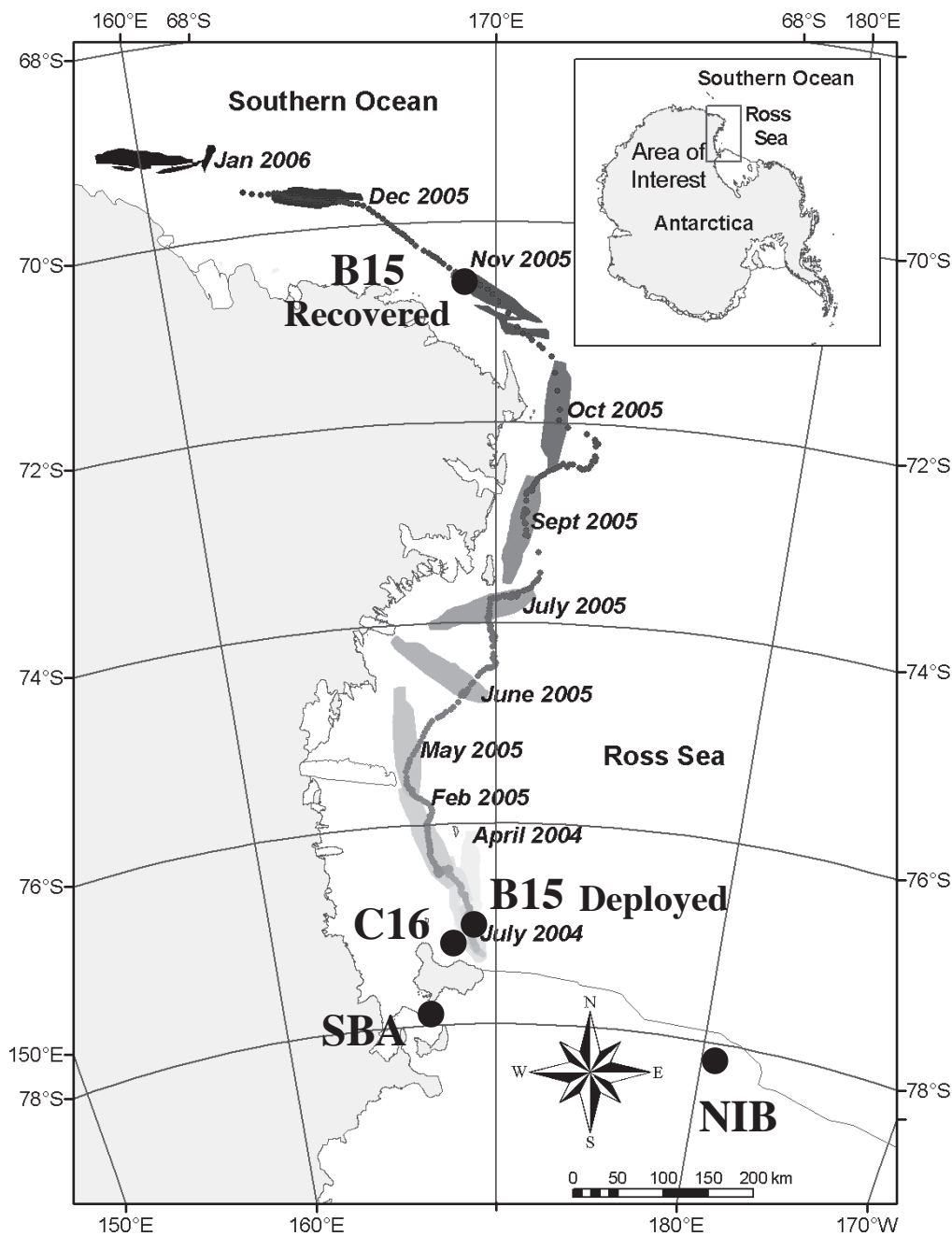
In this general context, the purpose of this paper is to report on the ancillary functioning of iceberg-sited seismometers as teleseismic observatories, and in particular their recording of the two Sumatra mega-earthquakes of 26 December 2004 and 28 March 2005. These data are available upon request from the authors.

We are in the third and final year of the SOUTHBERG deployment. In November–December 2003, we installed four seismic stations on iceberg C16 (including an STS-2 broadband instrument at the central station C16A) and left one of them to winter over during 2004. Because all stations work on solar power, the station shut down on 28 May 2004 after the arrival of permanent winter darkness at that latitude, but it woke up and started recording uneventfully on 25 September 2004 around the austral spring equinox, thus providing a total of 141 days of seismic recording, which went beyond our expectations. Bolstered by this performance, we left four stations to winter over in 2005: one at C16A (hereafter referred to as C16 for short), one on iceberg B15A, one on iceberg B15K (a fragment of B15A that detached in 2004), and one on the Ross ice shelf proper named "Nascent" or NIB because it is located immediately north of a crack where the next mega-iceberg is expected to calve off the shelf. Because B15A and B15K left their parking spots and started drifting during 2005, recovery of their instruments met with considerable logistical problems; recovery

could not be achieved at B15K, and this site may be visited in the future. The dataset analyzed in this paper thus consists of records at the three stations B15A (hereafter B15), C16, and NIB, mapped on figure 1, with relevant characteristics listed in table 1. One of the singular aspects of this experiment is that the seismic stations move as the icebergs drift; *e.g.,* the instrument at B15 was recovered 719 km from where it was deployed 357 days earlier. The data were recorded on two separate channels, sampled respectively at 1 Hz (SEED format LH*) and 100 Hz (SEED format HH*). Finally, we compared our seismic recordings with those of the permanent station SBA (Scott Base), which is part of the Global Seismic Network and located only 100 km from C16.

CHARACTERISTICS OF BACKGROUND NOISE

We first analyze the background noise recorded at the stations by the LH channels in the 0.1–10 mHz band. While its amplitude can fluctuate in particular as a function of meteorological conditions, we focus in figure 2(A) on a six-hour time window starting at 18:00 UT on 25 December 2004, *i.e.,* ending just before the Sumatra-Andaman earthquake, thus providing insight into the noise conditions during the recording of the event. We observe immediately that the iceberg stations are, of course, much noisier than SBA. This is not surprising because our seismometers simply are set on a slate in contact with the bulk of the iceberg, while SBA is installed on a pier attached to bedrock at the bottom of a 2-m-deep vault. The noise at B15 and C16 is generally of comparable amplitude, with C16 becoming slightly more noisy beyond 10 mHz. In contrast, NIB is quieter than the other two sites at frequencies below 0.6 mHz, but it becomes comparable to B15 between 10 and 50 mHz. In figure 2(B), we similarly examine the noise at higher frequencies, using a two-hour window of HHZ channels (BHZ at SBA), starting at 06:00 UT on 23 December 2004. Note that beyond 0.1 Hz, the four stations have essentially comparable noise amplitudes, which was not expected *a priori* given their different environments. Finally, note that all three iceberg sites show enhanced noise around 45 mHz ($T = 22$ s).

▲ **Figure 1.** Map of the SOUTHBERG experiment during the 2004–2005 season. The solid dots represent the locations of the stations (and, in black, of the permanent station SBA on Ross Island). The path of B15A's drift during 2004–2006 is shown by the small dots, plotted from daily GPS fixes, and by the silhouette of the iceberg in gray. Note its breakup in late October 2005.

These properties are generally interpretable in the context of the icebergs being tabular ice sheets, with the common thickness $h = 300$ m of the Ross ice shelf from which B15 and C16 calved away and of which NIB is still part. An elementary calculation shows that the natural period of an ice sheet of density ρ_i bobbing on water with density ρ_w is simply

$$T = 2\pi \sqrt{\left(\frac{\rho_i}{\rho_w}\right)\left(\frac{h}{g}\right)} \approx 33 \text{ s}$$

for $h = 300$ m. In the limit of a thin ice sheet, with transverse dimensions much greater than h, the pitching and rolling periods are expected to be $\sqrt{2}$ times shorter, or 23 s, close to the local maximum observed in the noise spectra. The generally larger amplitudes at C16 probably reflect the smaller size of the iceberg. Below 1 mHz, the origin of the background noise probably lies in microclimatic agents such as wind forcing, and the lower noise amplitude at NIB could stem from the other two stations sitting in the lee of vortices from Erebus volcano, as well as from the mechanical connection between the ice at

<table>

TABLE 1
SOUTHBERG Station Characteristics and Quantified Records, 2004–2005 Season

| | Iceberg Stations | | | |
	Nascent (NIB)	B15	C16	Reference Station
Coordinates upon deployment	−78.137; −178.510	−76.830; 168.730	−77.124; 167.900	**SBA:** -77.850; 166.800
Distance from SBA (km)	342	123	85	
Coordinates upon recovery	−78.127; −178.500	−70.386; 168.310	−77.052; 168.020	
Distance from SBA (km)	342	834	94	
Date of deployment	01 Nov (306) 2004	22 Nov (327) 2004	17 Nov (322) 2004	
Date of power shut-down	09 Apr (099) 2005	06 May (126) 2005	02 May (122) 2005	
Date of wake-up	26 Oct (299) 2005	06 Sep (249) 2005	16 Sep (259) 2005**	
Date of recovery	03 Nov (307) 2005	14 Nov (318) 2005	27 Oct (300) 2005	
Instrument Type	Güralp T-40	Güralp T-40	Güralp T-40	STS-1
Corner Frequency	33 mHz	1Hz	1Hz	
Sumatra-Andaman 2004: Rayleigh wave R_1				**SBA**
Spectral amplitude (Z; cm*s)	7.01	8.12	8.41	5.04
Equivalent M_m	8.11	8.16	8.16	7.94
Spectral amplitude (EW; cm*s)	1.82	1.65	2.42	3.03
Nias 2005: Rayleigh wave R_1				**SBA**
Spectral amplitude (Z; cm*s)	12.5	7.86	15.9	14.8
Equivalent M_{ms}	8.34	8.11	8.41	8.38
Spectral amplitude (EW; cm*s)	1.61	0.72	6.01	10.8
P waves: Parameter $\Theta = \log_{10} \dfrac{E^E}{M_0}$				**SBA**
Sumatra 2004	−5.64	−5.41	−5.37	−5.70
Residual to SBA	0.06	0.29	0.33	
Nias 2005	−5.09	−5.25	−5.48	−5.20
Residual to SBA	0.11	−0.05	−0.28	
Macquarie 2004	−4.89	−4.43	−4.57	−4.63
Residual to SBA	−0.26	0.20	0.06	
T phases: Eltanin 22 Dec (357) 2004				**RAR** **RPN**
Epicentral distance (km)	3,205	3,480	3,508	4,822 3,403
Parameter $\gamma = \log_{10}\left(\dfrac{\text{TPEF}}{M_0}\right) + 30$	1.65	1.78	2.29	3.40 2.76

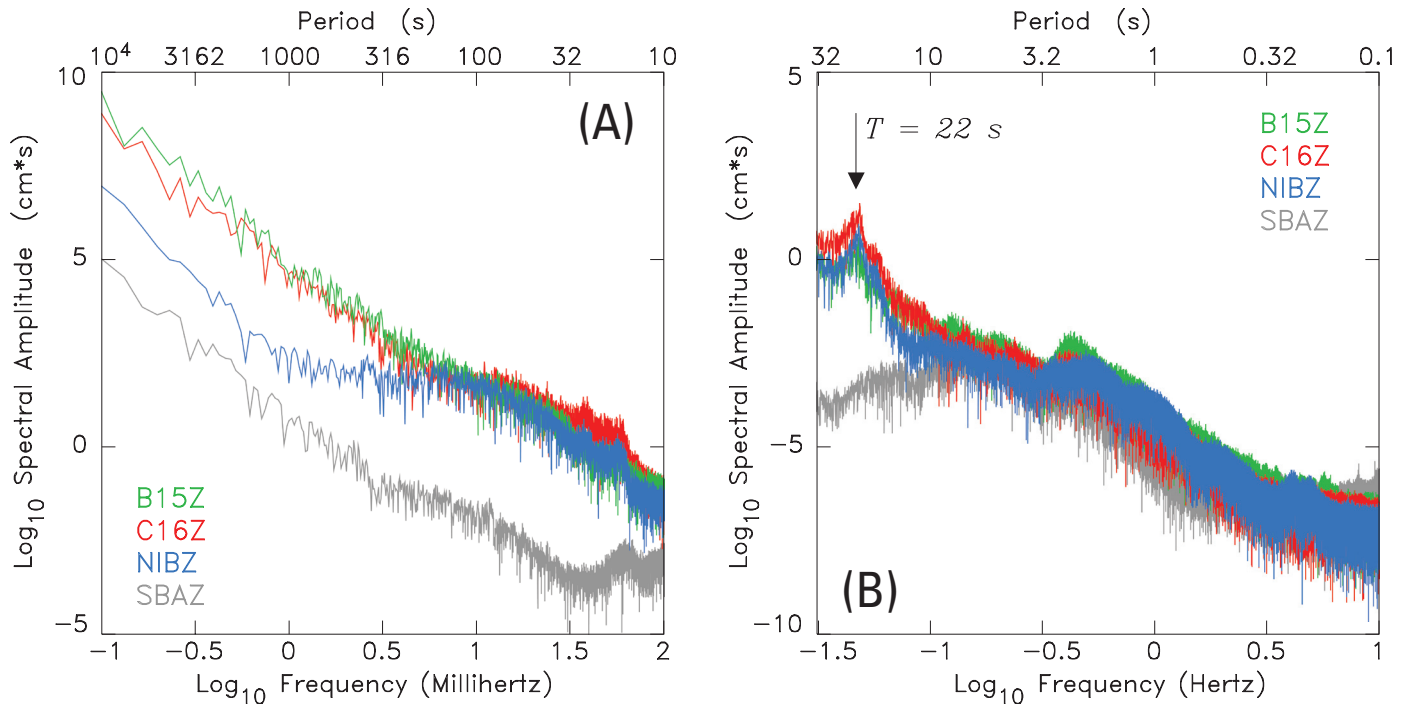** Station operated only intermittently between spring wake-up and recovery.
</table>

NIB and the whole Ross ice shelf (and eventually the Antarctic continent), which restricts its response to the forcing.

The noisy character of the stations has strong repercussions on their long-period detection capabilities. Figure 2 suggests minimum detectable spectral amplitudes on the order of 4 cm*s at $T \approx 20$ s at NIB and 330 cm*s at $T = 100$ s (as opposed to 6×10^{-3} and 0.08 cm*s, respectively, at SBA). Using the formalism of Okal and Talandier (1989) and Okal (1989), we find that this corresponds, in the case of surface waves at a distance of 90°, to moment thresholds of 2.5×10^{27} dyn*cm at 20 s, and 5×10^{29} dyn*cm at 100 s, meaning that mantle waves from the

2004 Sumatra earthquake should be barely if at all detectable. In contrast, we would expect that the iceberg stations should have detection capabilities at short periods comparable to those of SBA.

SEISMIC RECORDS OF THE SUMATRA EARTHQUAKES

We were fortunate that all three SOUTHBERG stations were operating during the Sumatra-Andaman earthquake of 26 December 2004 and the Nias earthquake of 28 March 2005.

▲ **Figure 2.** Comparison of background noise level as a function of frequency at the three SOUTHBERG stations and the nearby GSN station SBA (Scott Base). For each station, we plot the spectral amplitude of vertical ground motion analyzed over (A) a six-hour window starting at 18:00 UT on 25 December 2004 (LHZ channels) and (B) a two-hour window starting at 06:00 UT on 23 December 2004 (HHZ channels (BHZ at SBA).

In figure 3, we present spectrograms of the recording of the first event at NIB. As expected, the main Rayleigh wave R_1 is detectable only for periods $T \leq 50$ s, the second passage R_2 blends into the noise above 30 s, and only the largest aftershock (04:21 UT; $M_0 = 7.2 \times 10^{26}$ dyn*cm) is resolvable.

Quantification—Rayleigh waves

In table 1, we analyze quantitatively the spectral amplitudes $X(\omega)$ of the Rayleigh waves R_1 from both Sumatra earthquakes (26 December 2004 and 28 March 2005) as recorded at the three iceberg stations and compare them with their counterparts at the nearby station SBA. We use the mantle magnitude formalism of Okal and Talandier (1989) but restrict the study to $T = 51$ s, in view of the dominant noise at longer periods. On the vertical components, the iceberg stations perform very well: their average amplitudes are only 0.21 and 0.06 logarithmic units greater than at SBA for the 2004 and 2005 earthquakes, respectively. On the other hand, the east-west components (only 10° away from natural radial polarization) are significantly deficient at the iceberg stations. Whereas the land-based station SBA features ellipticity ratios of 0.60 and 0.73 respectively for the two events, in acceptable agreement with the classical theoretical value for the Rayleigh wave of a Poisson half-space (0.68), the horizontal spectral amplitudes at the iceberg stations fall to the noise level described above (1 cm*s).

All these results are easily explained using classical surface wave theory: The Rayleigh wave of a structure overlain by a liquid layer has no horizontal displacement at the free surface of the fluid, and the vertical displacement is essentially unper-

turbed if the thickness of the oceanic layer is much less than one wavelength (Haskell 1953). We have verified numerically that these results are unchanged by the addition of a layer of ice floating on the surface, with the horizontal component of the Rayleigh wave at the surface of the ice being two orders of magnitude smaller than at the top of the solid earth. Note finally that all mantle magnitude values at $T = 51$ s significantly underestimate the seismic moment of both earthquakes. This is an expression of the strong effect of source finiteness at that period, which is much shorter than the duration of either earthquake, but represents on the other hand the upper limit of the periods recording the Rayleigh wave above noise level. As expected, the ice stations did not record Love waves.
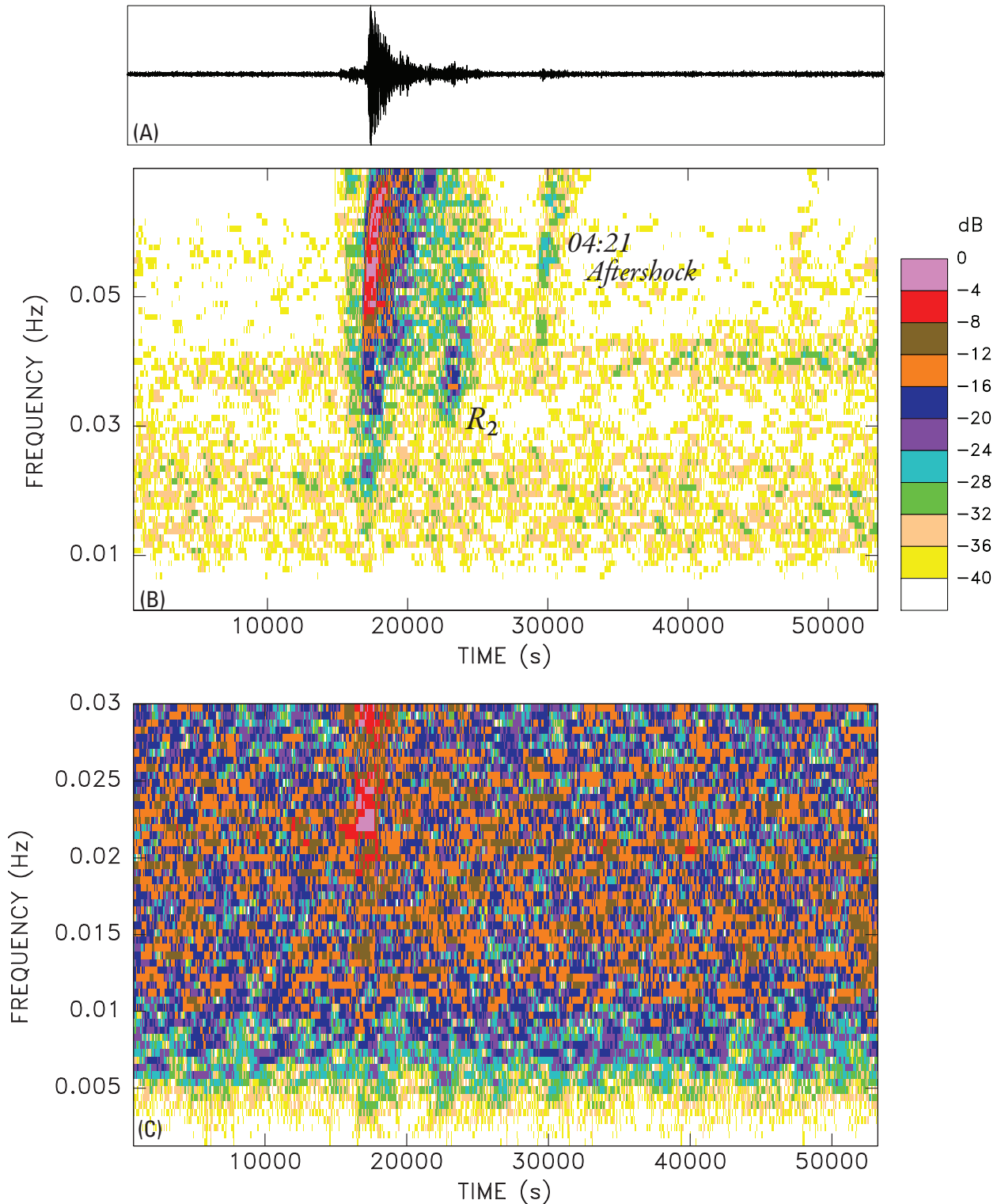
Quantification—*P* waves

Figure 4 shows that *P* waves from both Sumatra events are well-recorded on the HHZ channels. To quantify these records, we compute the estimated energy E^E and slowness parameter

$$\Theta = \log_{10} \frac{E^E}{M_0}$$

as defined by Newman and Okal (1998), and again compare their values with those obtained on the BHZ channel at the nearby station SBA. Because the epicentral distances (89° to 92°) fall outside the range for which Newman and Okal (1998) designed the algorithm, and in the case of the 2004 event because the exceptional duration of the source mixes the *P*-wavetrain
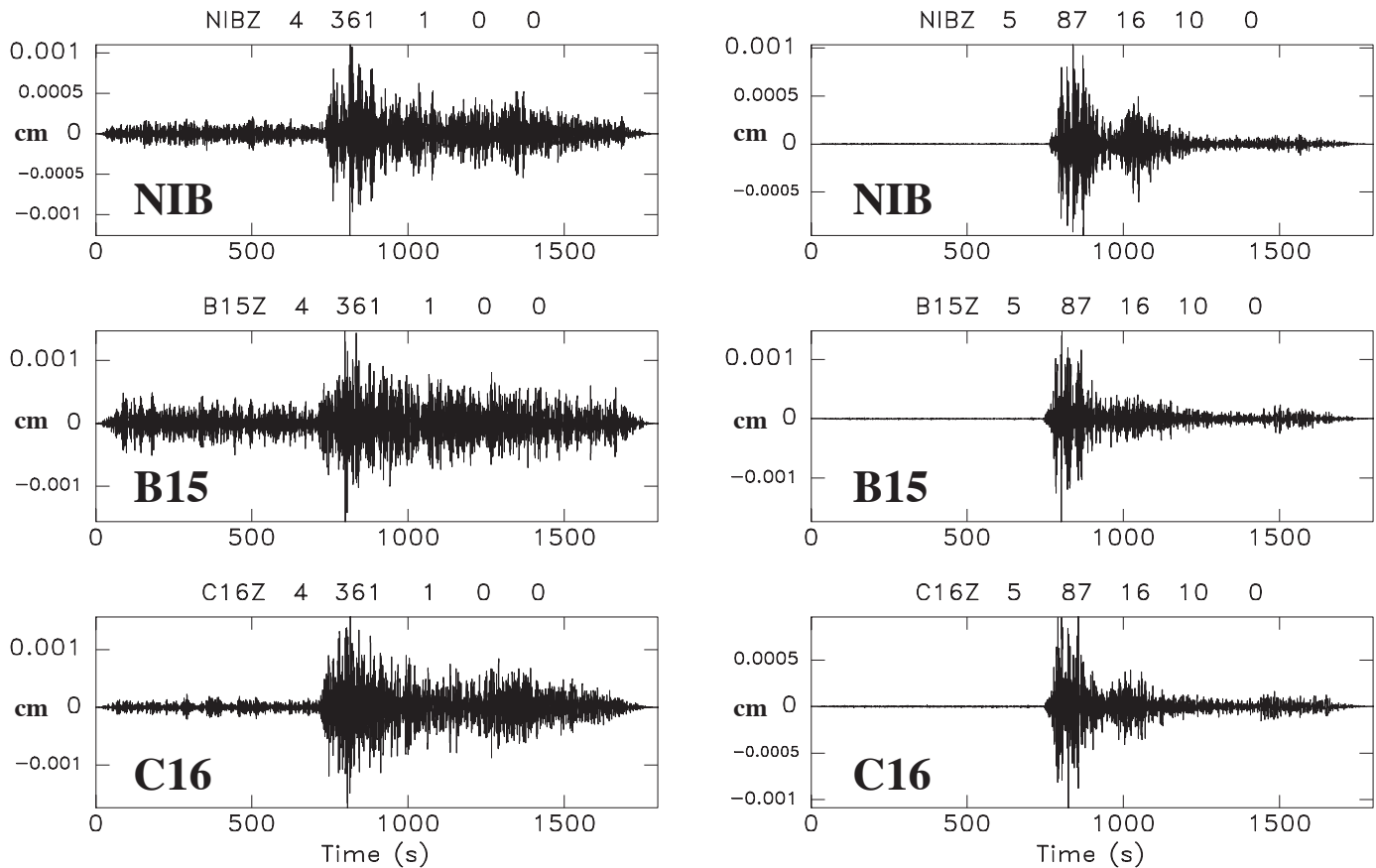
Nascent (NIB)—26 December 2004

▲ **Figure 3.** Vertical (LHZ) record of the 2004 Sumatra-Andaman earthquake at NIB. (A) Origin time series, starting at 18:00 UT on 25 December and running for 15 hours. (B) Spectrogram in the 1.5–70 mHz frequency band. (C) Close-up spectrogram in the 1.5–30 mHz frequency band. There is a 19 dB difference in absolute pixel intensity between (B) and (C). Note the main Rayleigh wave fading into the background noise around 10 mHz.

Sumatra-Andaman, 26 Dec. 2004

Nias, 28 March 2005

▲ **Figure 4.** *P*-wave arrivals recorded at the iceberg stations from the 2004 Sumatra and 2005 Nias earthquakes. Each frame is a 30-minute time series of the deconvolved vertical ground motion at the site, band-pass filtered between 0.1 and 10 Hz.

with later arrivals, only the relative values at the four stations can be considered. We find Θ values at the ice stations scattered −0.28 to +0.33 logarithmic units about the reference values at SBA, these numbers being typical of the scatter observed in large multistation datasets for a given earthquake (Newman and Okal 1998; Weinstein and Okal 2005). We also include an analysis of the large Macquarie earthquake of 23 December 2004, which preceded the Sumatra event by a few days ($M_0 = 1.6 \times 10^{28}$ dyn*cm), and which gives comparable results, even though the epicentral distances are in this case too short for the strict absolute application of the algorithm Θ.

We interpret our results as meaning that the vertical component of the *P* wave recorded on the ice is practically unperturbed with respect to its value at the top of the solid medium, even though the thickness of the water and ice system (~500 m) approaches the shortest wavelengths considered by the Θ algorithm (750 m at 0.5 s in the water).

HYDROACOUSTIC *T* PHASES

Figure 5 shows samples of hydroacoustic (*T*) phases detected by the SOUTHBERG stations from an earthquake on the Eltanin

transform fault (55.94°S; 125.00°W; $M_0 = 1.5 \times 10^{25}$ dyn*cm). This location was selected because it offers a direct unmasked great circle path to the SOUTHBERG stations. Because the nearby station SBA, masked by Ross Island, did not record the *T* phase, we use the stations at Rarotonga, Cook Islands (RAR), and Easter Island (RPN) as references. At each station we proceed to compute the so-called *T*-phase energy flux (TPEF) and scale it to the seismic moment of the earthquake, M_0, through the parameter
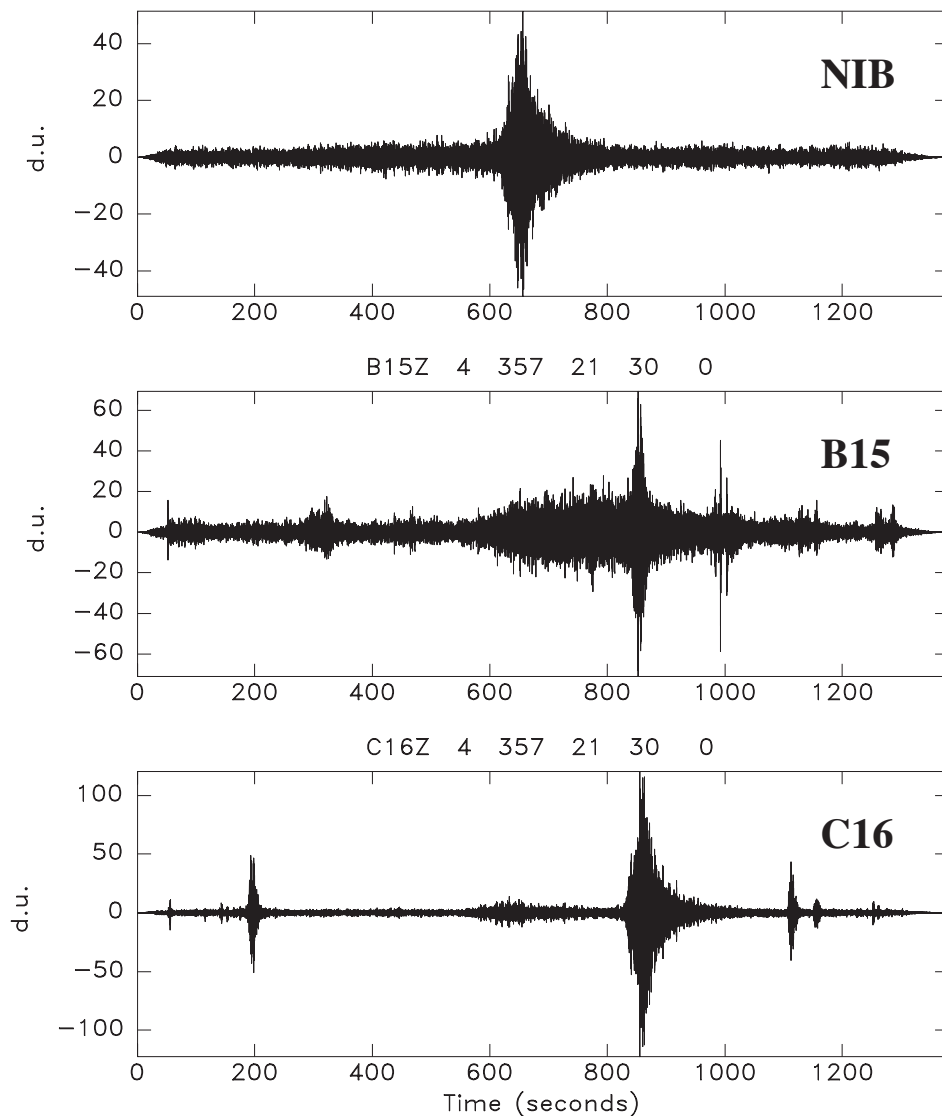
$$\gamma = \log_{10}\left(\frac{\text{TPEF}}{M_0}\right) + 30 \qquad \text{(using c.g.s. units).}$$

These parameters were introduced by Okal *et al.* (2003) and Okal (2006a) to offer a quantitative characterization of the strength of teleseismic *T* phases at island stations. Because of the strong dependence of *T* phases on the details of the acoustic-to-seismic conversion at the receiving shore, γ should in principle be used only to compare *T* phases at the same receiver and from events arriving at comparable azimuths (Okal *et al.* 2003). In particular, and for this reason, their computation involves no

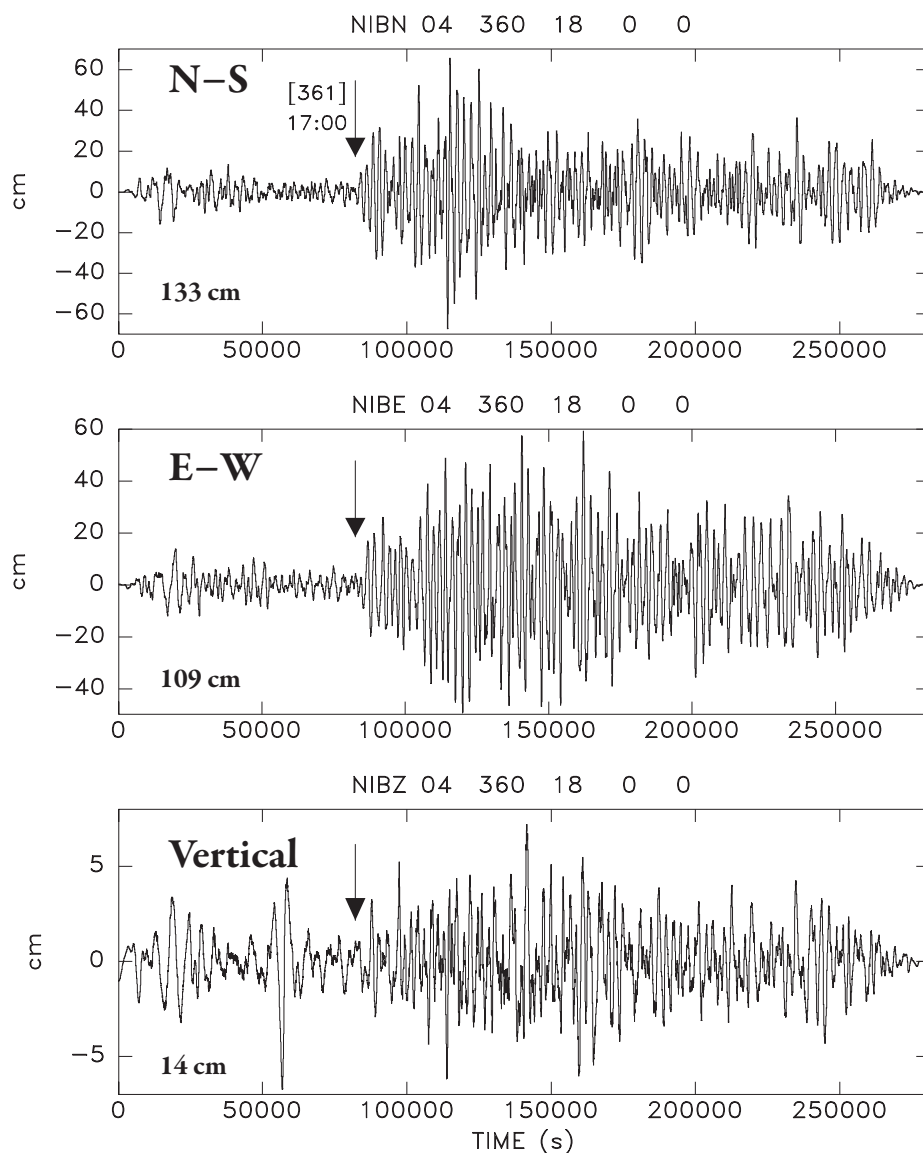# *T* Phases from Eltanin Event
22 DECEMBER 2004

▲ **Figure 5.** *T* phases recorded at the iceberg stations from the Eltanin transform fault earthquake of 22 December 2004. The time windows are 23 minutes long and start at 21:30 UT. They represent HHZ channels, band-pass filtered between 2 and 10 Hz. Note the stronger amplitude at C16 and the background activity on the two floating icebergs, including a long window of tremor at B15.

distance correction. Here, we propose to use this concept to grossly quantify the icebergs as receivers of *T* phases.

The values of γ listed in table 1 show that the icebergs record the *T* waves at a somewhat weaker level than typical volcanic islands located at comparable epicentral distances. This very preliminary observation may be rooted in the deformation of the acoustic wave in the very shallow water of the Ross Sea, where the acoustic channel coincides with the entire, although narrow, water column, or in the details of the acoustic-seismic coupling at the water-ice interface. The slightly higher TPEF observed at C16 may reflect a physical contact between the ice mass and the solid earth, which could act as a preferred scatterer for the conversion.

These results are important because they provide some insight, through the principle of seismic reciprocity, into the mechanism by which hydroacoustic waves can be generated by sources located inside the icebergs. We emphasize that despite several studies (Talandier *et al.* 2002, 2006; Chapp *et al.* 2005), we do not understand well the nature of such so-called "cryosignals," but at least this study proves that seismic-acoustic conversions are possible between the icebergs parked along the shores of the Ross Sea and the body of water in the Southern Ocean. Furthermore, our γ values suggest that such conversions could be somewhat less efficient than those occurring on the slopes of typical small volcanic islands such as Rarotonga or Easter.

Seismic recordings of 2004 Sumatra Tsunami
Nascent (NIB); *26 DECEMBER 2004*

▲ **Figure 6.** Three-component recording of the 2004 Sumatra tsunami by the SOUTHBERG station NIB. These time series start seven hours before the earthquake and last 78 hours. They represent deconvolved ground motion, band-pass filtered between 0.1 and 10 mHz. The peak-to-peak amplitude for each component is given at bottom left in the corresponding frame.
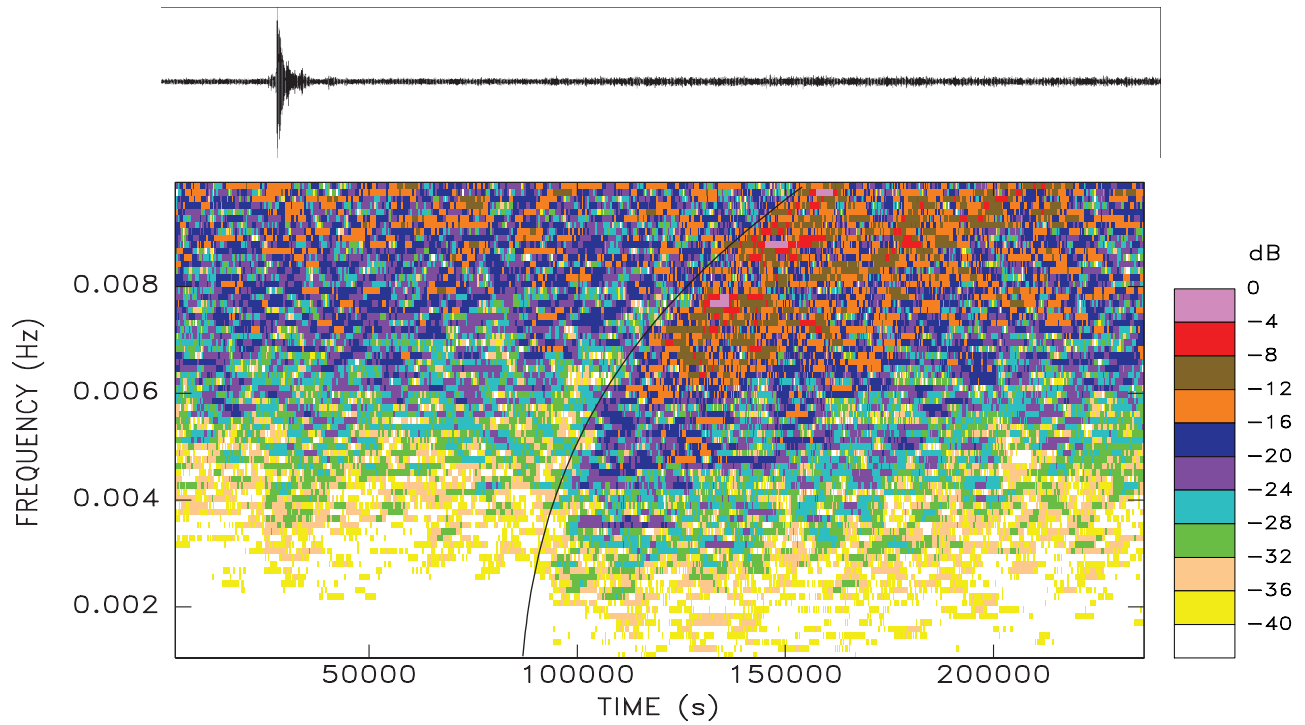
SEISMIC RECORDS OF TSUNAMIS

Next, we examine the records obtained at the SOUTHBERG stations of the tsunami generated by the 2004 Sumatra earthquake. In a landmark paper, Yuan *et al.* (2005) reported that seismic stations located in the immediate vicinity of island or continental shorelines in the Indian Ocean recorded the impact of the 2004 tsunami on their horizontal components, an observation confirmed by Hanson and Bowman (2005). Okal (2006b) later generalized these observations worldwide (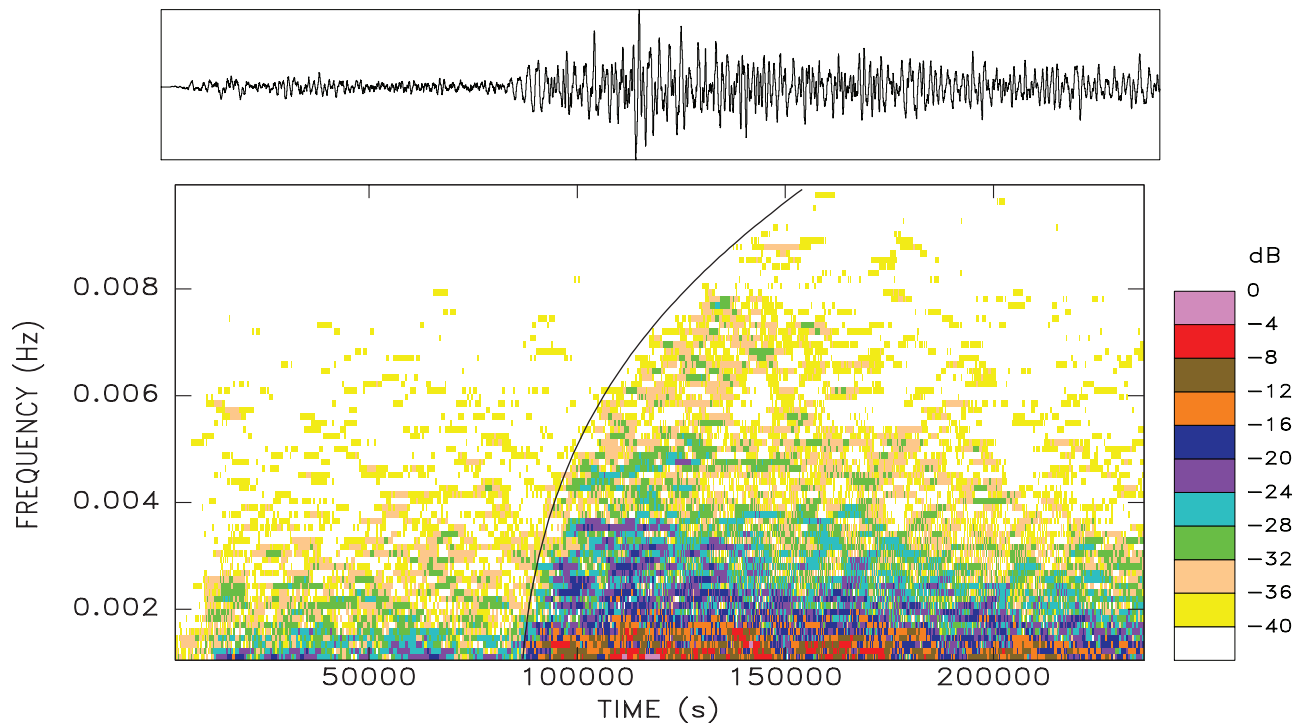including at SBA) and showed that they could be quantified under the extreme simplifying assumption that the seismometer was acting as an ocean-bottom instrument in the absence of the island structure. We show here that the SOUTHBERG seismic stations provided the unique opportunity to directly record the motion of the ocean due to the tsunami.

As documented in figure 6, NIB recorded the tsunami on all three components, starting 16 hours after origin time. The spectrograms in figure 7 show a clear dispersion of the arrival, characteristic of propagation outside the shallow water approximation, as previously described on hydroacoustic and seismic records of the tsunami by Hanson and Bowman (2005) and

(A) NIB—26 DEC 2004—Vertical Raw Record

(B) NIB—26 DEC 2004—North-South Ground Motion

▲ **Figure 7.** Spectrograms of the 2004 Sumatra tsunami recorded at NIB. (A) Raw record of the vertical component. (B) Deconvolved ground motion from the north-south component. In both frames, the solid black line is the theoretical dispersion curve for a distance of 11,800 km over an ocean of average depth 3.8 km.

Okal *et al.* (2006). This observed dispersion is best-fit by propagation along 11,800 km over an ocean of depth 3.8 km, such values being reasonable for the somewhat convoluted path of the tsunami around Australia and Antarctica. The high-frequency part of the wave train ($f \geq 5$ mHz) was also well-recorded at B15 and C16, but the difference in instrument response at those two stations acted to filter out the lower frequency components beyond detection. The deconvolved seismograms in figure 6 show peak-to-peak amplitudes of 14 cm on the vertical component and 133 cm on the north-south component, expected to be in the general direction of arrival of the wave. The former value compares favorably with Titov *et al.*'s (2005) peak-to-peak amplitude of 10.5 cm at a virtual gauge located at their southernmost grid point (71°S, 170°E), which is, however, 850 km away. The aspect ratio of the deconvolved ground motion is on the order of 10, in remarkable agreement with its value predicted under the shallow-water approximation

$$\frac{u_x}{u_z} = \frac{1}{\omega}\sqrt{\frac{g}{h}}$$

which would vary between 4 at 500 s in a 4-km-deep sea and 22 at 1,000 s in a 500-m-deep sea, more representative of the local bathymetry in the Ross Sea. We conclude that the seismometer at NIB responded to the three-component displacement of the surface of the ocean under the tsunami. In particular, this is fundamentally different from the response of a land-based seismometer (such as at SBA), which, as shown by Okal (2006b) based on the theory of Gilbert (1980), responds to a combination of horizontal displacement and tilt of the solid ocean bottom (plus a small gravitational term). If the solid iceberg had exactly followed the local motion of the sea surface, then it would have deformed and Gilbert's (1980) theory would similarly predict a compensation (which would become perfect under shallow-water asymptotics) between the displacement and tilt terms of the response of the horizontal seismometer, while that of the vertical instrument would be largely unaffected. In this framework, we note that at a typical period of 500 s, the wavelength of the tsunami in the Ross Sea is only 35 km, which is much smaller than the dimension of the ice shelf. The strong signal on the horizontal component at NIB then leads us to surmise that the iceberg (or ice shelf) may have responded to the tsunami by following the displacement of the water surface more or less as a rigid body, without deforming to reproduce the exact field of tilt expected along the free surface of the ocean. Results at the other two stations, B15 and C16, were generally similar but restricted to higher frequencies in view of their different instrument response.

Finally, we were able to detect a tsunami signal at NIB from the large earthquake of 23 December 2004 near Macquarie Island with a vertical peak-to-peak amplitude of 2.3 cm and a horizontal one of 17 cm (figure 8). The deconvolved spectral amplitude at $T = 80$ s, $X(\omega) = 1,250$ cm*s, would translate into $M_{TSU} = 8.23$, using the formalism of Okal and Titov (2006), or $M_0 = 1.7 \times 10^{28}$ dyn*cm, in excellent agreement with the Harvard CMT solution of 1.6×10^{28} dyn*cm, which confirms that tsunami records at this ice station are representative of the amplitude of the wave on the high seas despite the presence of a large continental shelf in the Ross Sea. In addition, this represents a rare example of generation of a far-field tsunami by a strike-slip earthquake, as predicted theoretically by Ward (1980) and Okal (1988). (Because the Sumatra tsunami did not propagate to our stations over a great circle, it was not possible to run the M_{TSU} algorithms on its records.)

By contrast, the tsunami from the 2005 Nias earthquake was not detectable above the noise level at any of the three stations.

RECORDING OF STORM WAVES FROM DISTANT METEOROLOGICAL DEPRESSIONS

Figures 9(A) and 9(B) show an example of the recording at SOUTHBERG stations of storm waves of meteorological origin starting on 27 October 2005 and lasting 514,134 s or 6.5 days (station C16 was already pulled out at the time). The strongly dispersed branch corresponds to deep water waves, whose apparent slope of frequency versus arrival time is directly related to range Δ through

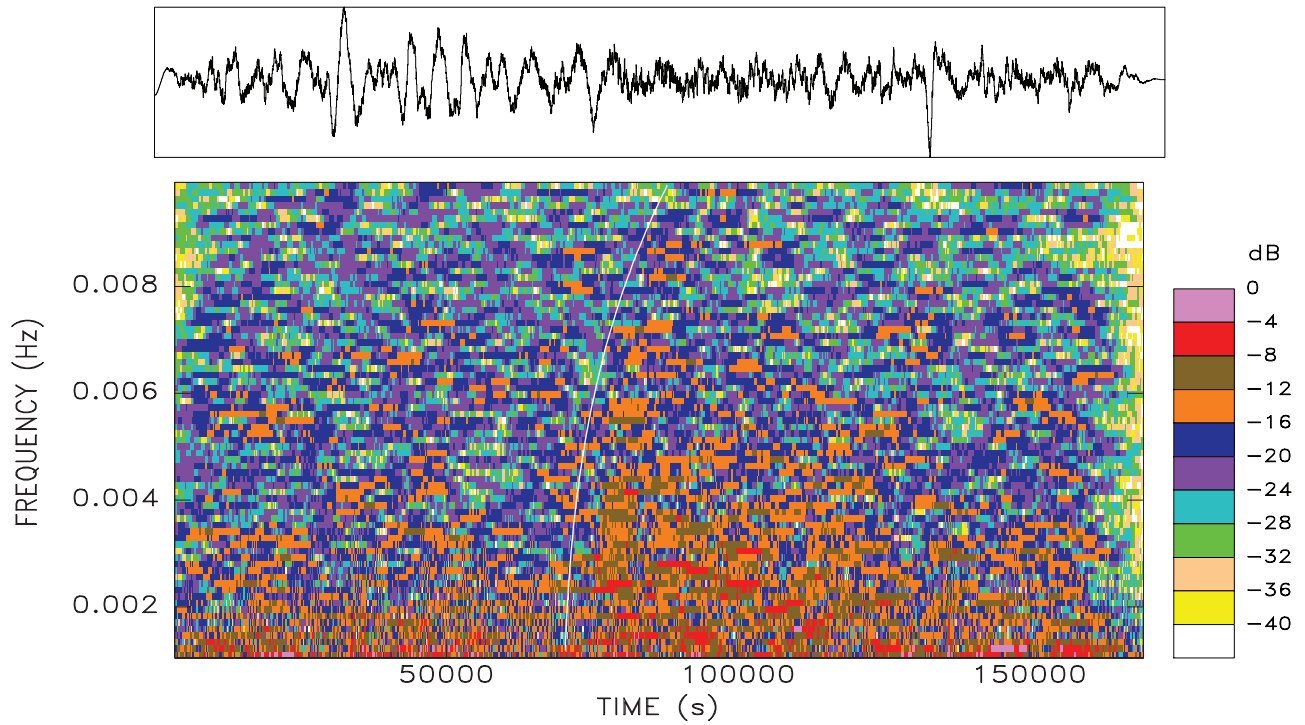$$\frac{df}{dt_{arr}} = \frac{1}{\Delta} \cdot \frac{g}{4\pi}$$

suggesting a source at a distance $\Delta = 14,000$ km. We verified that a severe storm was present in the Gulf of Alaska (47°N, 155°W) on 21 October 2005, the waves of which took six days to reach the Ross Sea, and confirmed this interpretation using the records at the intermediary station PTCN located on the small island of Pitcairn. Figure 9(C) documents a comparable dispersion in the 30–60 mHz window but with a steeper slope corresponding to the shorter distance of 8,400 km; note also that the storm arrives 2.5 days earlier at Pitcairn than in Antarctica. Such recordings have been described previously at ground stations (*e.g.*, Munk *et al.* 1963; Snodgrass *et al.* 1966; Barruol *et al.* 2006). We document in figure 9 the classical nonlinear response of the small island of Pitcairn, resulting in the generation of a strong harmonic at double the frequency of the fundamental sea swell (Longuet-Higgins 1950; Hasselmann 1963), which is absent from the records at the ice stations. As expected, the amplitudes of ground motion in the relevant frequency bands are much larger on the ice (120–150 μm peak-to-peak on both vertical and horizontal components) than at PTCN (0.6 μm and 3 μm peak-to-peak for the fundamental and the harmonic, respectively).

An additional remarkable aspect of our observations is that they correlate in time with the breakup of iceberg B15A, which took place precisely on 27 October 2005, leading to legitimate speculation about the possible role of the storm waves in triggering the breakup (MacAyeal *et al.* 2006).
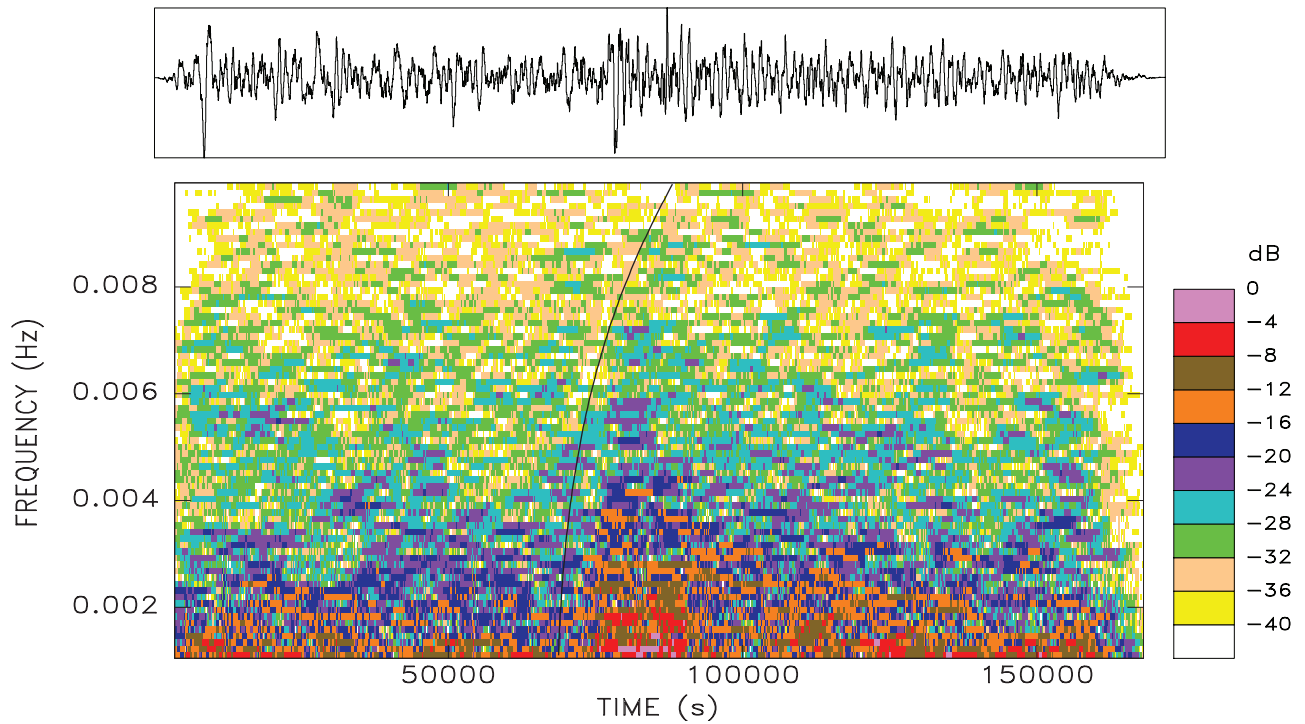
CONCLUSION

We have shown that seismometers deployed on parked or drifting mega-icebergs floating in the Ross Sea can function as teleseismic receivers, but that their performance is affected by sub-
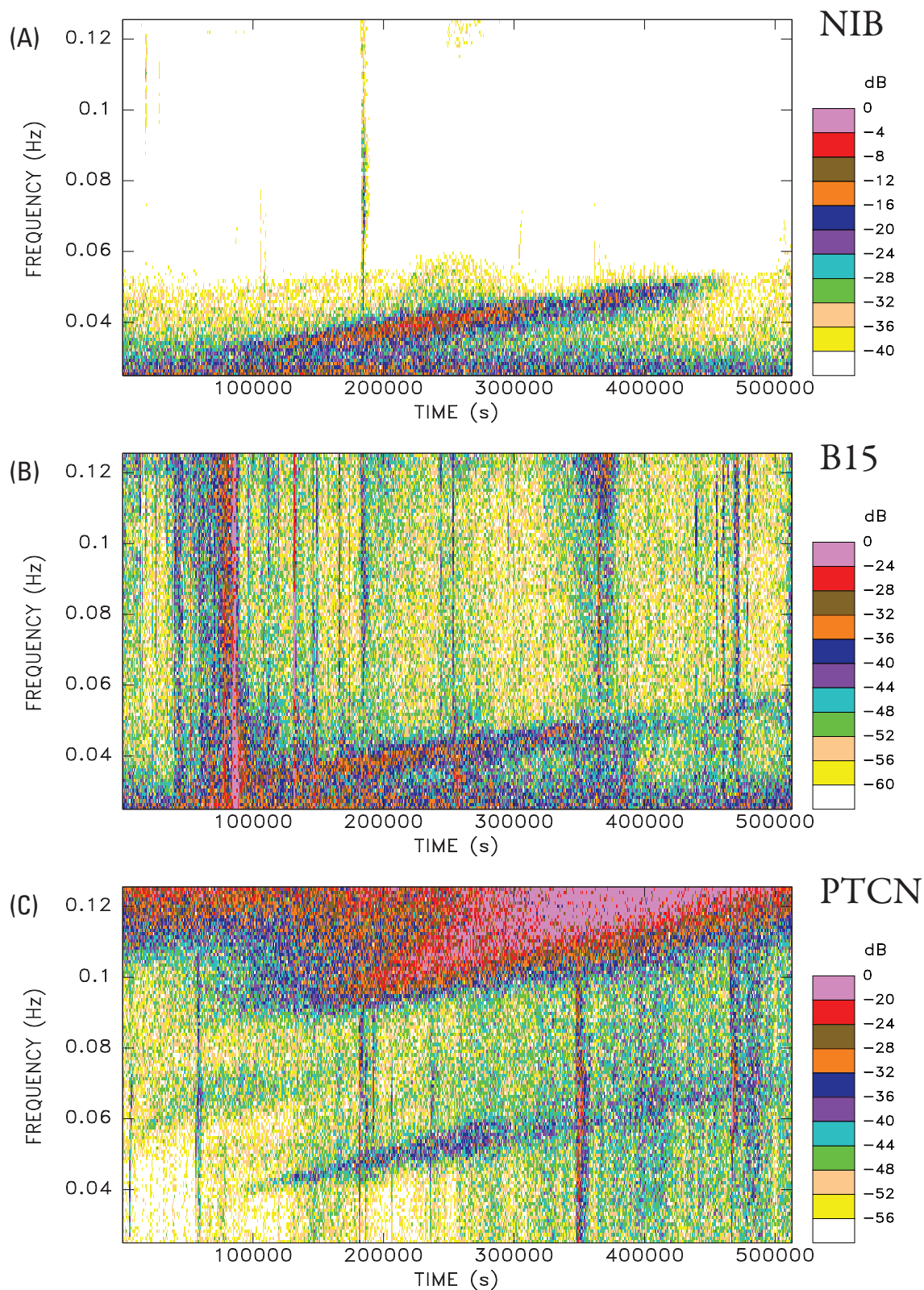
(A) NIB— 23 DEC 2004 (Macquarie)—Vertical

(B) NIB—23 DEC 2004 (Macquarie)—North-South

▲ **Figure 8.** Spectrograms of the small tsunami generated by the Macquarie earthquake of 23 December 2004, as recorded at NIB, on (A) the vertical and (B) north-south components. In both instances, the records have been deconvolved to ground motion. The thick lines (white and black, respectively) show the dispersion expected for propagation over a 3.5-km deep ocean.

▲ **Figure 9.** Spectrograms of storms recorded at the iceberg stations (A) NIB and (B) B15, and at (C) Pitcairn Island. Each frame represents a 142.8-hour time window, starting at 01:16 on 27 October 2005 (SOUTHBERG stations) or 03:45 on 25 October 2005 (PTCN). Note the strong dispersion, the slope of which allows the computation of distance under the deep-water approximation. The ice stations are recording the fundamental wave in the frequency band 30–55 mHz, while in addition the ground station prominently displays the harmonic resulting from nonlinear conversion at the shore.

stantial noise below 0.1 Hz, notably in the bandwidth of the natural frequencies of oscillation of the bergs on the seawater. Otherwise, our quantification of teleseismic body and surface waves from the two large Sumatra events of 2004 and 2005 shows that the sites respond as predicted theoretically for layered structures in the presence of a fluid, namely that vertical ground motion is practically unaffected by the shallow layers of water and ice but the horizontal ground motion signal is lost at the decoupled interface between the ocean and the solid earth. Our recording of the 2004 Sumatra tsunami at the sites is in general quantitative agreement with numerical simulations in the open ocean and suggests that the icebergs were entrained as passive rafts during the oscillations of the ocean surface, without evidence of deformation of the ice mass itself. The recording of hydroacoustic waves following a moderate earthquake on the Pacific-Antarctic Ridge confirms the coupling of the ice masses to the oceanwide SOFAR channel, as previously hinted following the observation of ice tremors in the teleseismic hydroacoustic spectrum. Finally, we show that icebergs are influenced by distant weather in the form of deep water waves generated by severe storms at the other end of the Pacific Basin. ▰

ACKNOWLEDGMENTS

REFERENCES

Barruol, G., D. Reymond, F. R. Fontaine, O. Hyvernaud, V. Maurer, and K. Maamaatuaihutapu (2006). Characterizing swells in the southern Pacific from seismic and infrasonic noise analyses. *Geophysical Journal International* **164**, 516–542.

Chapp, E., D. R. Bohnenstiehl, and M. Tolstoy (2005). Sound-channel observations of ice-generated tremor in the Indian Ocean. *Geochemistry, Geophysics, and Geosystems* **6**, Q06003, 14 pp.

Gilbert, F. (1980). An introduction to low-frequency seismology, in *Proceedings of the International School of Physics Enrico Fermi,* A. M. Dziewonski and E. Boschi, eds. (Amsterdam: North Holland).

Hanson, J. A., and J. R. Bowman (2005). Dispersive and reflected tsunami signals from the 2004 Indian Ocean tsunami observed on hydrophones and seismic stations. *Geophysical Research Letters* **32** (17), L17606, 5 pp.

Haskell, N. A. (1953). The dispersion of surface waves on multilayered media. *Bulletin of the Seismological Society of America* **43**, 17–34.

Hasselmann, K. (1963). A statistical analysis of the generation of microseisms. *Reviews of Geophysics* **1**, 177–210.

Longuet-Higgins, M. (1950). A theory of the origin of microseisms. *Philosophical Transactions of the Royal Society of London, Series A* **243**, 2–36.

MacAyeal, D. R., E. A. Okal, R. C. Aster, J. N. Bassis, K. M. Brunt, L. M. Cathles, R. Drucker, H. A. Fricker, Y.-J. Kim, S. Martin, M. H. Okal, O. V. Sergienko, M. P. Sponsler, and J. E. Thom (2006). Transoceanic wave propagation links iceberg-calving margins of Antarctica with storms in tropics and Northern hemisphere. *Geophysical Research Letters* **33** (17), L17502, 4 pp.

Munk, W. H., G. R. Miller, F. E. Snodgrass, and N .F. Barber (1963). Directional recording of swell from distant storms. *Philosophical Transactions of the Royal Society of London, Series A* **255**, 505–584.

Newman, A. V., and E. A. Okal (1998). Teleseismic estimates of radiated seismic energy: The E / M_0 discriminant for tsunami earthquakes. *Journal of Geophysical Research* **103**, 26,885–26,898.

Okal, E. A. (1988.) Seismic parameters controlling far-field tsunami amplitudes: A review. *Natural Hazards* **1**, 67–96.

Okal, E. A. (1989). A theoretical discussion of time-domain magnitudes: The Prague formula for M_s and the mantle magnitude M_m. *Journal of Geophysical Research* **94**, 4,194–4,204.

Okal, E. A. (2006a). The generation of T waves by earthquakes. *Advances in Geophysics* **49**, forthcoming.

Okal, E. A. (2006b). Seismic records of the 2004 Sumatra and other tsunamis: A quantitative study. *Pure and Applied Geophysics,* forthcoming.

Okal, E. A., and J. Talandier (1989). M_m: A variable period mantle magnitude. *Journal of Geophysical Research* **94**, 4,169–4,193.

Okal, E. A., and V. V. Titov (2006). M_{TSU}: Recovering seismic moments from tsunameter records. *Pure and Applied Geophysics*, forthcoming.

Okal, E. A., P.-J. Alasset, O. Hyvernaud, and F. Schindele (2003). The deficient T waves of tsunami earthquakes. *Geophysical Journal International* **152**, 416–432.

Okal, E. A., J. Talandier, and D. Reymond (2006). Quantification of hydrophone records of the 2004 Sumatra tsunami. *Pure and Applied Geophysics*, forthcoming.

Snodgrass, F. E., G. W. Groves, K. F. Hasselmann, G. R. Miller, W. H. Munk, and W. H. Powers (1966). Propagation of oceanic swell across the Pacific. *Philosophical Transactions of the Royal Society of London, Series A* **259**, 431–497.

Talandier, J., O. Hyvernaud, E. A. Okal, and P.-F. Piserchia (2002). Long-range detection of hydroacoustic signals from large icebergs in the Ross Sea, Antarctica. *Earth and Planetary Science Letters* **203**, 519–534.

Talandier, J., O. Hyvernaud, D. Reymond, and E. A. Okal (2006). Hydroacoustic signals generated by parked and drifting icebergs in the Southern Indian and Pacific Oceans. *Geophysical Journal International* **165**, 817–834.

Titov, V. V., A. B. Rabinovich, H. O. Mofjeld, R. E. Thomson, and F. I. Gonzalez (2005). The global reach of the 26 December 2004 Sumatra tsunami. *Science* **309**, 2,045–2,048.

Ward, S. N. (1980). Relationships of tsunami generation and an earthquake source. *Journal of Physics of the Earth* **28**, 441–474.

Weinstein, S. A., and E. A. Okal (2005). The mantle wave magnitude M_m and the slowness parameter Θ: Five years of real-time use in the context of tsunami warning. *Bulletin of the Seismological Society of America* **95**, 779–799.

Yuan, X., R. Kind, and H. Pedersen (2005). Seismic monitoring of the Indian Ocean tsunami. *Geophysical Research Letters* **32** (15), L15308, 4 pp.

Department of Geological Sciences
Northwestern University
1850 Campus Drive
Evanston, Illinois 60208
emile@earth.northwestern.edu
(E.A.O.)

Department of the Geophysical Sciences
University of Chicago
5734 South Ellis Avenue
Chicago, Illinois 60637
drm7@midway.uchicago.edu
(D.R.M.)